The Separation Behavior of Impurities in the Purification of High-Purity Magnesium via Vacuum Distillation

Neng Xiong[1] · Semiramis Friedrich[1] · Seifeldin R. Mohamed[1] · Ivan Kirillov[1] · Xiaozhou Ye[1] · Yang Tian[2,3] · Bernd Friedrich[1]

Abstract

Magnesium-based materials with exceptional properties are being widely used in the automotive and aerospace industries, as well as in electronic equipment and Mg-based implants. The development of many advanced engineering structures and precision devices prompts the demand for high-purity Mg with better performance and service. However, the current purification methods meet challenges such as the complex equipment, potential dangers due to the powdery condensed products, and the lack of systematic analysis of the impurity behavior. Here, we report the purification of commercial raw materials into 99.9958% (± 0.0034%) pure magnesium products through one-step vacuum distillation. The process adopts a vertical distillation device, which has the advantages of high recovery efficiency, lumpy condensation products, easy cleaning, and reusability. Experimental results confirm that vacuum evaporation is more effective than vacuum sublimation for the purification of magnesium. Then, the behavior of eight impurities is analyzed theoretically and experimentally. The results significantly verify the difficulty sequence of impurity separation from the Mg base, which is $Zn > Ca > Pb > Al > Cu > Ni$. The similar equilibrium vapor pressure of Zn and Mg and the separation coefficient close to unity are the reasons that cause zinc to be the most difficult one to be separated.

Graphical Abstract
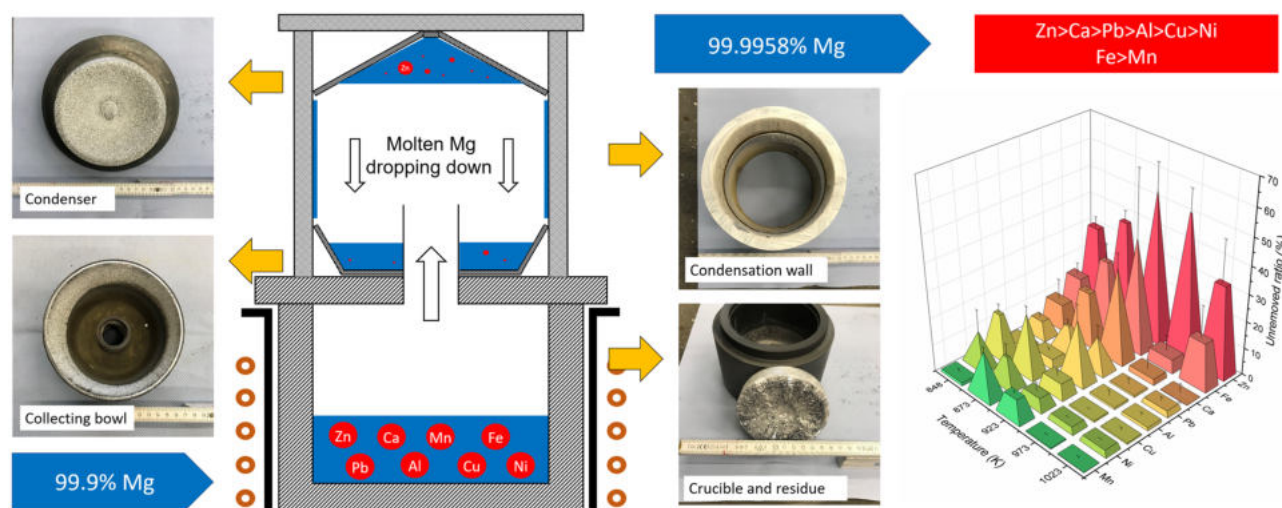
Neng Xiong and Semiramis Friedrich have contributed equally to this work.

The contributing editor for this article was Adam Clayton Powell.

Extended author information available on the last page of the article

Introduction

High-purity grade magnesium is utilized in the preparation of magnesium-based materials that are increasingly employed in a wide range of automobile and aerospace industries [1], electronic devices [2], and Mg-based implants [3]. Recent significant growing attention to various applications of Mg-based materials is attributed to its superior properties, such as low density [4], high specific strength [5], strong electromagnetic shielding ability [6], high thermal [7] and electrical conductivity [8], high dimensional accuracy and stability [9], as well as good extrudability [10], and biocompatibility [11].

Recently, the corrosion resistance has attracted great attention because it limits the application of Mg-based materials under fairly mild exposure conditions, such as indoor (and outdoor) atmospheric exposure [12]. The poor corrosion resistance of Mg is due to the weak protection of the natural surface films and micro-galvanic corrosion acceleration from second phases [13]. The elements that from these second phases usually have a strong cathodic behavior in the materials, which leads to the formation of micro-cells that cause serious corrosion, and subsequently hinder the prolongation of service life of the materials [14]. To be specific, the existence of trace impurities (with higher exchange current density for hydrogen reduction, such as Cu, Al, Ni, Zn, Fe, and Mn) provides more favorable places for the cathodic reaction [15, 16]. All the above studies have indicated that the systems of Mg and other elements corrode faster than high-purity Mg (HP-Mg). Thus, with controlling impurities below the tolerance limit [15], these high-purity alloys can exhibit better corrosion resistance in comparison to the normal ones. The performance of high- and ultra-high-purity magnesium (HP-Mg and UP-Mg) and its alloys is expected to be improved.

There are currently two routes to commercially produce primary magnesium: electrolysis [17] and thermal, such as Pidgeon process [18] and vacuum carbothermal reduction process [19]. The electrolysis process accounts for the majority of the Western world's production capacity, and commercial applications of thermal processes are concentrated in China. These methods are used to produce primary Mg with a purity level between 99.8% and 99.98% (2N8–3N8) [20]. And then, in order to meet the demand for high-performance Mg-based materials, many methods are used to increase the purity level of primary magnesium [20–23]. Among these techniques, vacuum distillation has the advantages of high impurity removal efficiency, few processes, low energy consumption, and environmental friendliness [24].

HP-Mg products have been successfully fabricated by vacuum distillation using different experimental equipment. However, the systematic research and application of primary magnesium purification are still having potential problems, specifically due to the following three aspects. Firstly, it is known that the purity level is calculated by 100% minus the total concentration of all impurities, while some purity results come from few elements detection [25] and low measurement accuracy [26, 27]. If the regulatory limit of the detection element is lower than or close to the lower detection limit of ICP-OES, ICP-MS will be the instrument of better choice [28, 29]. Second challenge is the low efficient recovery of condensed magnesium. Using similar equipment, two patents have showed that the purity of magnesium is increased to 5N purity via vacuum distillation [30, 31]. However, collecting the condensed Mg and cleaning the inner chamber encounter difficulties due to the complicated structure of the apparatus. As most of the condensation products are fine powders, they are easily to be oxidized and with the risk of explosion [32]. Finally, the researches lack theoretical support and analysis of impurity behavior. The experimental investigations have reported that ultrapure products can be obtained via vacuum distillation [30, 33, 34]. However, among these few available documents, the purity level has only been improved through the equipment modification. In particular, the reason why the impurity zinc is more difficult to be removed has not been explained. Some results are even obtained after ignoring the concentration of zinc. Therefore, to the best of our knowledge, based on the effective detection methods and devices, theoretical analysis and experiments on the change of behavior for sufficient detectable impurities in HP-Mg have not been systematically carried out.

In this paper, we study the theoretical separation situations of eight impurities (Zn, Ca, Pb, Mn, Al, Cu, Fe, and Ni) from Mg base by the criteria of the equilibrium vapor pressure, the separation coefficient β, the gas–liquid equilibrium diagram, and the solubility. Then, we investigate the influence of experimental parameters on the distillation process. The paper devotes chiefly to clarify the behavior of impurities in magnesium purification. The experimental part of this study has been conducted at IME Process Metallurgy and Metal Recycling, The Institute of RWTH Aachen University and the theoretical calculation at Kunming University of Science and Technology. This research is to provide the basis for the sustainable development of the production of HP-Mg.

Methods

Theoretical Analyses

Equilibrium Vapor Pressure

A theoretical basis for the use of vacuum distillation to achieve the separation of different components is the equilibrium vapor pressure of different substances. Under a given system pressure, as the temperature increases, the component with higher vapor pressure will be more easily volatilized and separated from the initial material. The relationship between the equilibrium vapor pressure and temperature of an element can be expressed as [35]

$$\lg p^* = AT^{-1} + B\lg T + CT + D, \tag{1}$$

where p^* is the equilibrium vapor pressure, Pa; T is the temperature, K; and A, B, C, and D are the evaporation constants [36].

Separation Coefficient β and Gas–Liquid Equilibrium Diagram

Due to the presence of complex inter-particles forces between the different elements present in the base metal matrix, the individual vapor pressure could only serve as a preliminary indicator to the behavior of these impurities. Therefore, a parameter called the separation coefficient β is introduced for a more accurate evaluation of the separation effect [35]:

$$\beta_i = \frac{P^*_i \cdot \gamma_i}{P^*_{\text{Mg}} \cdot \gamma_{\text{Mg}}}, \tag{2}$$

where P^*_i and P^*_{Mg} are the equilibrium vapor pressures of impurity i and Mg at a given temperature, respectively; and γ_i and γ_{Mg} are the activity coefficients of impurity i and Mg at a given temperature, respectively; and β_i is the separation coefficient of impurity i. When $\beta_i > 1$, impurity i is volatilized before Mg, while it is vice versa at $\beta_i < 1$. And when $\beta_i = 1$, it means that the separation of the impurity from magnesium is difficult to achieve.

The main challenge usually facing this model is the calculation of the activity coefficient, as the value varies with the temperature of the system and the initial concentration of each impurity. To simplify the challenge of this model, it is assumed that the magnesium part is an infinite dilute solution with no individual impurity exceeding 1% concentration, which means γ_{Mg} could be taken as unity. On the other hand, the infinite dilution activity coefficient

of the individual impurity can be calculated according to the following equation [35]:

$$\ln \gamma_i^\infty = \frac{\bar{H}_i^{\text{E}\infty}}{RT} - \frac{\bar{S}_i^{\text{E}\infty}}{R}, \tag{3}$$

where γ_i^∞ is the activity coefficient; R is the ideal gas constant, 8.314 J/mol·K; T is the thermodynamic temperature, K; $\bar{H}_i^{\text{E}\infty}$ is the partial molar excess enthalpy, J·mol^{-1}; and $\bar{S}_i^{\text{E}\infty}$ is the partial molar excess entropy, J·mol^{-1}·K^{-1}. Equation (3) is based on the assumption that the partial molar excess entropy and partial molar excess enthalpy of a substance do not change with the temperature. Then, the separation coefficient β_i can be generated by combining Eqs. (1)– (3).

The separation tendency between magnesium and its impurities can also be illustrated through the gas–liquid equilibrium diagram. When an impurity in magnesium reaches an equilibrium state, the relationship between the impurity concentrations in the gas phase (g) and the liquid phase (l) can be expressed by the following formula [35]:

$$i_{\text{g}} = \left(1 + \frac{\text{Mg}_{\text{l}}}{i_{\text{l}}} \cdot \frac{\gamma_{\text{Mg}}}{\gamma_i} \cdot \frac{P^*_{\text{Mg}}}{P^*_i}\right)^{-1}, \tag{4}$$

where Mg_{l}, i_{l}, and i_{g} are the concentrations of Mg and the impurity in the liquid and gas phase, respectively. For theoretical calculation, the initial concentration of impurity i in Mg is assumed to be 1–100 ppm (points at 1, 5, 10, 50, 100 are selected).

Solubility

It is known that the introduction of the activity coefficient is to make the thermodynamic formula of the ideal solution applicable to the real solution. However, no thermodynamic data of the elements Mn and Fe for calculating the activity coefficient can be found in [37]. According to the Mg–Mn and Mg–Fe systems, they are dominated by the wide region of immiscibility in the liquid phase. That means, Mn or Fe can hardly dissolve in Mg, impeding thermodynamic data obtaining of the melt. Therefore, the modules of "Phase diagram" and "Equilib" in FactSage 8.0 software are used to analyze the dissolution of Mn and Fe in the Mg-rich base. Here, the solubility results are calculated via "Equilib" module in the FactSage 8.0 software.

Experimental Procedures

In each group of trails, approximately, 450 g of magnesium (99.9 wt%, supplied by Magontec GmbH, Germany) was used as raw material for vacuum distillation. The trails were conducted in a vacuum induction furnace (40 kW maximum

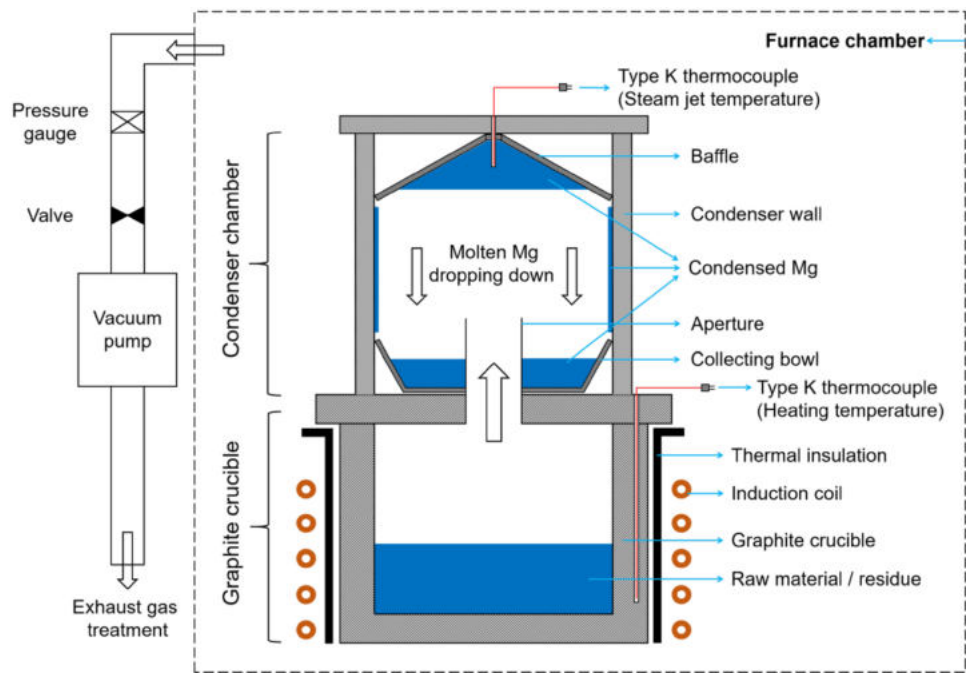**Fig. 1** The cross-sectional view of the structure of the distillation device

Table 1 Parameters of all vacuum distillation experiments

No. of trails	Temperature (K)	Holding time (min)	Pressure (Pa)
1–3	848	120, 150, 180	18
4–6	873		85
7–10	923	30, 45, 60, 90	100
11–14	973		140
15–18	1023		400

power, 4 kHz maximum frequency, 1873 K maximum temperature). Figure 1 shows the sketch of the vacuum distillation setup, with the bottom heating part served by a high-purity graphite crucible ($\Phi = 150$ mm, $h = 155$ mm) and the upper cooling part made of steel ($\Phi = 150$ mm, $h = 200$ mm). The setting temperature and actual temperature were calibrated after the setup being surrounded by the coil (Fig. S1 and Fig. S2, Supplementary Material). Before being placed in the graphite crucible for distillation, all surfaces of the raw materials were mechanically ground and cleaned in an ethanol ultrasonic bath to remove the oxide layer and minimize foreign contaminants.

The parameters of conducted trails are listed in Table 1. After the system pressure reached around 10 Pa, the temperature was raised to the target point at a rate of 45 K/s. During the process, the volatilized gaseous magnesium entered into the cooling part through the aperture and subsequently condensed in the condenser chamber (the baffle, the condenser wall, and the collecting bowl). The partial pressure of gaseous magnesium increased during the distillation process, which could be higher than the system pressure. The system pressure was adjusted to a certain value for different holding temperatures. After the holding time accomplished, the induction system was turned off, and the distillation setup was freely cooled to the ambient temperature. Especially, due to the poor volatility of the 873 K-experimental group, the holding times at this temperature were extended to 120, 150, and 180 min. And in order to verify the result reliability of this group, an additional 848 K comparison group at same holding times was performed.

Under the pressure conditions of this study, the volatilization of magnesium included two processes: evaporation and sublimation [38]. The specific surface area changed significantly with the pressure of the system. Therefore, the volatilization rate was not analyzed in this study. Finally, Inductively Coupled Plasma Mass Spectrometry (ICP-MS, triple quadrupole, Agilent 8900) was used to analyze the raw materials and samples were collected from the baffle, the condenser wall, and the collecting bowl. Multi-point sampling was performed to ensure the accuracy of the analysis results.

After the experiments, the evaporation ratio (E) is to be calculated as:

$$E = \frac{m_{\text{raw}} - m_{\text{residue}}}{m_{\text{raw}}} \times 100\%, \tag{5}$$

where m_{raw} and $m_{residue}$ are the mass of the raw material and the residue in crucible, respectively. The calculation of the loss ratio (L) for distillation process is

$$L = \frac{m_{raw} - m_{residue} - m_{recovery}}{m_{raw}} \times 100\%, \quad (6)$$

where $m_{recovery}$ is the mass of recovered Mg from the condenser chamber, including the baffle, the condenser wall, and the collecting bowl. The calculation of the recovery ratio (R_c) for evaporated Mg is

$$R_c = \frac{m_{recovery}}{m_{raw} - m_{residue}} \times 100\%. \quad (7)$$

The unremoved ratio (U_i) is used to reflect the removal level of individual impurities via vacuum distillation methodology. It is calculated as

$$U_i = \frac{C_{ic}}{C_{ir}} \times 100\%, \quad (8)$$

where C_{ir} and C_{ic} are the concentrations of the impurity i of the raw material in the crucible and condensed Mg from the cooling part, respectively.

Results and Discussion

The Theoretical Analysis of Mg in the Vacuum Distillation Process

Figure 2 shows the variation of equilibrium vapor pressure of different elements with the temperature. The display of some missing line segments is because for Formula (1), each element has its own limited temperature range (Table S1, Supplementary Material). It can be seen that the order of volatile elements is Zn > Mg > Ca > Pb > Mn > Al > Cu > Fe > Ni. Under given conditions, Mg and Zn will be firstly volatilized and separated from other elements in the residue. Thus, the major reason for purifying magnesium via vacuum distillation is the sequence of volatilization between the elements, leading to the separation feasibility. In addition, compared with the application of vacuum distillation of other metals, magnesium shows advantages in its distillation

conditions. The critical equilibrium vapor pressure to distinguish, whether magnesium is vaporized or sublimated, is 333 Pa [38], which is a vacuum condition that can be achieved without high costs or big efforts.

The calculation results of the separation coefficients of impurity i at different temperatures are listed in Table 2. As it can be seen, the values of β_{Zn} are close to unity, which demonstrates the difficulty of zinc and magnesium separation. Other metals can achieve better separation effects with $\beta_i \ll 1$. Figure 3 shows the gas–liquid equilibrium diagrams of Mg-i (i = Zn, Ca, Pb, Al, Cu, or Ni) binary systems. Being very close to the absolute values of the concentration of zinc in the liquid as well as gas phase, Fig. 3a indicates again the challenge of its removal from magnesium base. In contrast, other impurities are basically concentrated in their liquid phase when they reach the gas–liquid equilibrium state (see Fig. 3b–f). Comparing the impurity concentration in the gas and the liquid phase, the difficulty of separating the impurity from the magnesium base is obviously Zn > Ca > Pb > Al > Cu > Ni.

As shown in Fig. 4, the Mg–Mn and Mg–Fe phase diagrams indicate that there are no compounds in the system. On the other hand, the calculation results of solubility (Table S2, Supplementary Material) verify the weak
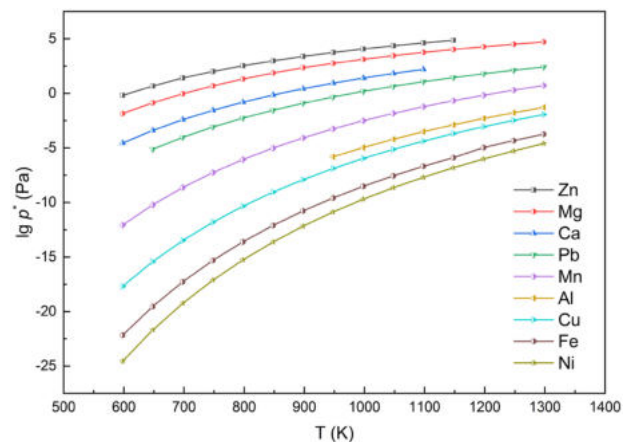

Fig. 2 The equilibrium vapor pressure of elements Zn, Mg, Ca, Pb, Mn, Al, Cu, Fe, and Ni in the temperature range of 600–1300 K

Table 2 The separation coefficients of impurities at different temperatures

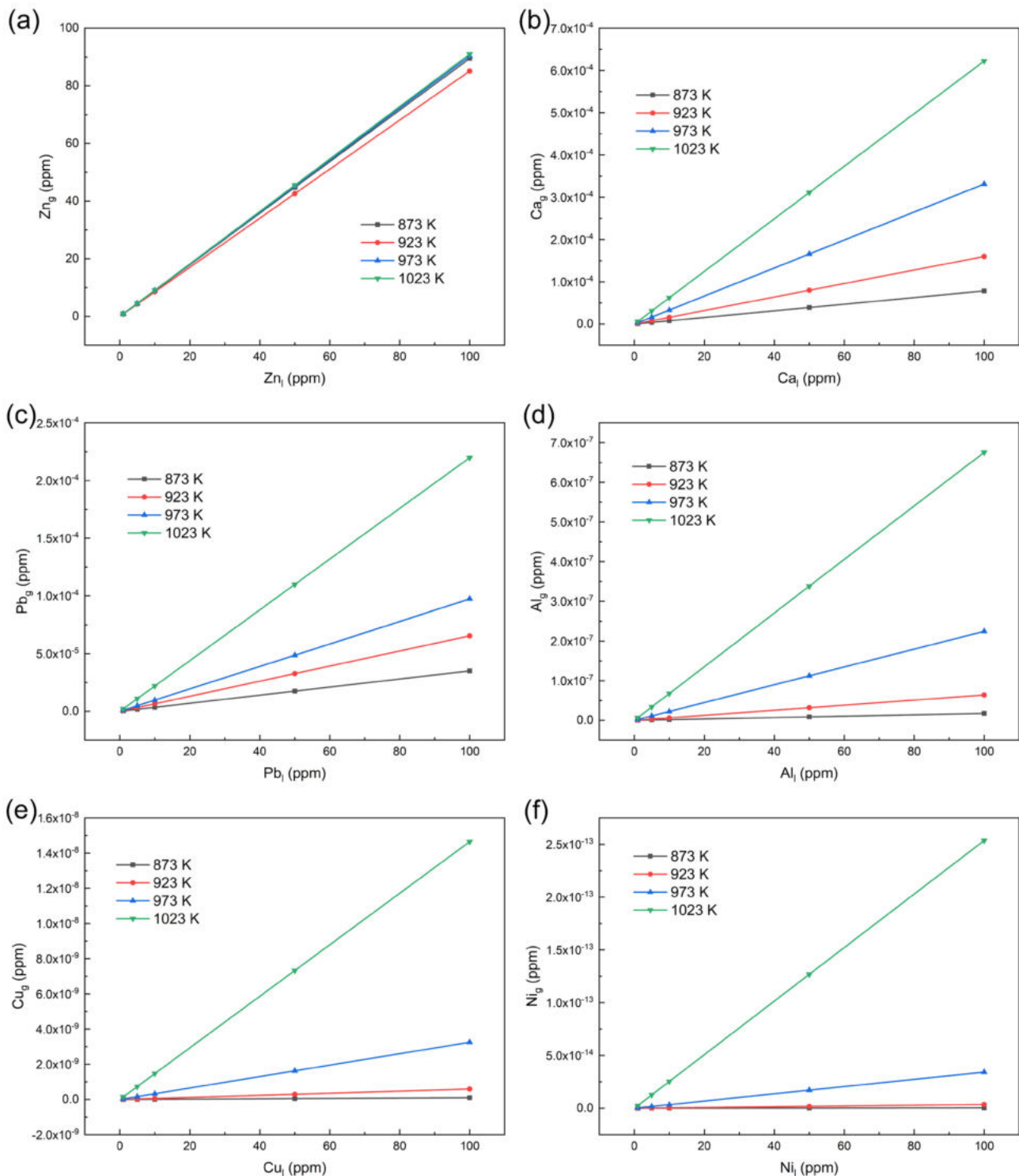| Temperature (K)	873	923	973	1023
β_{Zn}	8.945×10^{-1}	8.514×10^{-1}	9.031×10^{-1}	9.100×10^{-1}
β_{Ca}	7.836×10^{-7}	1.560×10^{-6}	3.314×10^{-6}	6.223×10^{-6}
β_{Pb}	3.503×10^{-7}	6.544×10^{-7}	9.735×10^{-7}	2.198×10^{-6}
β_{Al}	1.750×10^{-10}	6.384×10^{-10}	2.245×10^{-9}	6.758×10^{-9}
β_{Cu}	9.783×10^{-13}	5.892×10^{-12}	3.249×10^{-11}	1.465×10^{-10}
β_{Ni}	3.207×10^{-18}	3.564×10^{-17}	3.418×10^{-16}	2.536×10^{-15}

Fig. 3 The gas–liquid equilibrium diagrams of impurities **a** Zn, **b** Ca, **c** Pb, **d** Al, **e** Cu, and **f** Ni in Mg-*i* binary systems, respectively

dissolution of Mn and Fe in the Mg-rich base. Under the setting conditions of 1023 K and 400 Pa, Mn and Fe reach the maximum solubility, which are 0.0326% and 0.0008%, respectively. The solubility result fits well with the situation shown in the phase diagram. That is, Fe is more difficult to dissolve in Mg-rich base than Mn. Due to the difference in criteria, Mn and Fe cannot be compared with the impurities mentioned earlier.
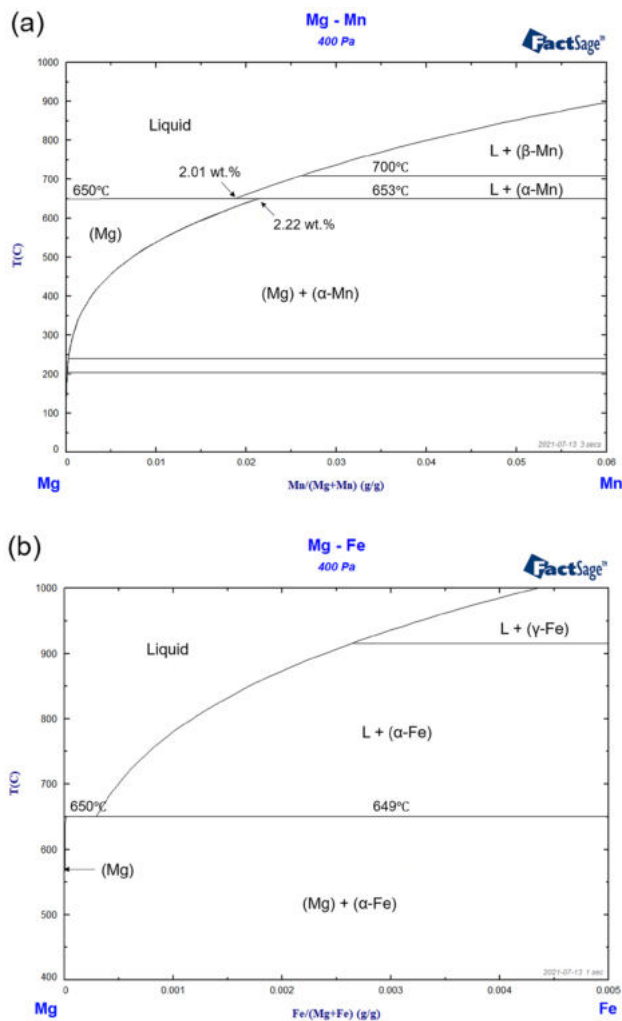
Fig. 4 The phase diagram of **a** Mg–Mn and **b** Mg–Fe systems

## The Evaporation Behavior of Mg in the Vacuum Distillation Process

Figure 5 shows the cross-sectional view of the structure of the distillation device and different parts of the distillation setup after accomplishment of a trial. It can be seen that most of the cooled product is accumulated by the baffle on the top (A). The vertical condenser wall (B) and the collecting bowl (C) collect a small part of the metal vapor. The main condensed material on the baffle can be easily collected even without the use of any tools and be removed by hand wearing latex gloves as it has a very low adhesion to the boron-nitride coating of the steel baffle. The other part of the collected material is in the collecting bowl after solidification of those molten droplets, falling down from the baffle or the wall. Also for the collection of this part, no tools are required. That means, no scraping or scratching of the powdery product is needed, which

would commonly lead to oxidation of magnesium. The easy-to-collect condensed product and the maximum loss ratio of 4.20% (Table S3, Supplementary Material) illustrate that the setup can effectively realize the distillation and the condensation processes. Compared to the more complicated equipment [30, 31, 33], the distillation setup shows the advantages of simple structure, easy cleaning, and reusability.

As shown in Fig. 6a, the evaporation ratio obtained at one constant temperature increases with the holding time, as well as increases with the heating temperature at a constant holding time. Although the sublimation processes (848 K- and 873 K-groups) have longer holding times, the evaporation processes (923 K-, 973 K-, and 1023 K-groups) show a greater volatilization efficiency. In addition, the evaporation ratios of the 973 K- and 1023 K-groups are close to each other, and both higher than the 923 K-group. After reaching 923 K, a slight increase (50 K) in the heating temperature will no longer significantly increase the evaporation ratio of magnesium. On the other hand, the recovery ratios of all groups are between 95.60% and 102.23% (see Fig. 6b), which is not significantly affected by the heating temperature and the holding time. In the actual operation, the value of $m_{recovery}$ has been calculated by weighing the whole condenser chamber before and after the distillation. The weighing error is caused by the insulation material outside the device, resulting in the partial recovery ratio to be higher than 100%. The maximum evaporation ratio (96.00%) and recovery ratio (95.60%) are reached under the heating temperature of 1023 K and a holding time of 90 min.

Due to the different condensation locations and unclear condensation period in the process, it is difficult to measure the condensation temperature directly. The steam jet temperature, means the temperature directly above the aperture, being increased by "thundering" the hot magnesium vapor/steam. Longer holding times lead to higher steam jet temperature, because more Mg-vapor comes out. The steam jet temperature is a secondary parameter, which is influenced by the main process parameters such as crucible temperature, pressure, and time. This temperature has no direct influence on the purification efficiency and impurities removal, as it has been shown in this study. Table S3 (Supplementary Material) shows steam jet temperature for every combination of process parameter. The steam jet temperature range from the baffle is 863–913 K, which is higher than the reported condensation temperatures [25–27, 30]. A slightly higher temperature in the condensation zone than the theoretical condensation temperature of magnesium will result in a condensation product with larger grain size [38], which is beneficial to the subsequent collection of magnesium products.

Fig. 5 The cross-sectional view of the structure of the distillation device (middle part), and physical pictures of the baffle (A), the condenser wall (B), the collecting bowl (C), the crucible, and the residue (D) of a trial
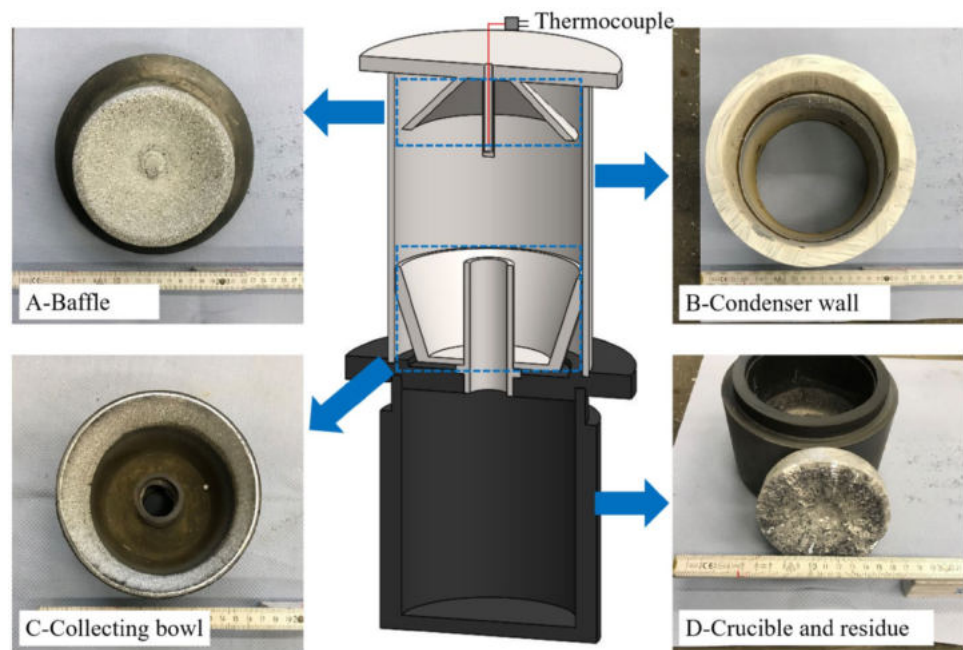
The Impurity Behavior in the Purification of Mg via Vacuum Distillation

The analysis shows that there is not much difference in the purity of Mg collected from the baffle, the condenser wall, and the collecting bowl after the same experiment. Thus, the final concentration of the impurity is calculated as the average of the detection results at these three locations. The concentrations of all impurities in the raw material and magnesium condensates are listed in Table 3. Except for one experimental group (923 K–90 min), the purity of the magnesium product obtained in all other 17 groups has reached 99.9958% ($\pm$0.0034%). The 3N pure initial raw materials can be purified to reach the purity of 4N8 (848 K–150 min, 973 K–45 min, 973 K–90 min, 1023 K–60 min) and even 5N (1023 K–45 min). Comparing with the published experimental parameters and results, this study has advantages not only in the distillation setup, but also in terms of feedstock scale, vacuum feasibility, and reproducibility of high-purity products (Table S4, Supplementary Material). Moreover, inconsistent with the view that the condensation products obtained in the higher temperature region have a higher purity [39, 40], there is no significant relationship between the steam jet temperature and the purity in this study.

Figure 7 shows the "unremoved ratio" of eight impurities (Zn, Fe, Ca, Pb, Al, Cu, Ni, and Mn) at different temperatures. The setting of the "unremoved ratio" (Y axis) in the 3D image is in order to an obvious exhibition of the removal efficiency of each impurity. The deviation is calculated from the difference between the minimum and the average unremoved ratios in multiple experiments of one temperature. It

reflects the deviation of the removal efficiency of the individual impurities at each temperature, which confirms the effectiveness of the detection method. For impurities Ca, Pb, Al, Cu, Ni, and Mn, 973 K- and 1023 K-groups show higher impurity removal ratio and smaller deviation compared with other heating temperatures. This is all of course with the exception of the impurity zinc. It also indicates that vacuum evaporation is better than vacuum sublimation when removing impurities.

All impurities are arranged according to the average removal efficiency. With an average unremoved ratio of 41.70% (Table S5, Supplementary Material), zinc possesses the most difficult impurity position, completely consistent with the theoretical analysis results. The separation coefficient of zinc—close to unity—also makes it difficult to be separated from magnesium base by the two-step vacuum distillation method. It means that after the initial separation of zinc and magnesium from other elements, further vacuum distillation is no longer effective for the separation of zinc and magnesium. In terms of the average unremoved ratio, the order of difficulty in removing impurities from the magnesium base is Zn > Fe > Ca > Cu > Ni > Pb > Al > Mn, while the order derived from the separation coefficient β criterion and the gas–liquid equilibrium diagram is Zn > Ca > Pb > Al > Cu > Ni. It should be noticed that two impurities with low concentration in the raw material, Cu (2.00 ppm) and Ni (0.47 ppm), are reduced to the detection limit (0.01 ppm) (see Table 3). From the perspective of detection limit, these two impurities are considered to be the easiest to remove. Excluding the other two special elements Fe and Mn that cannot be applied to theories of
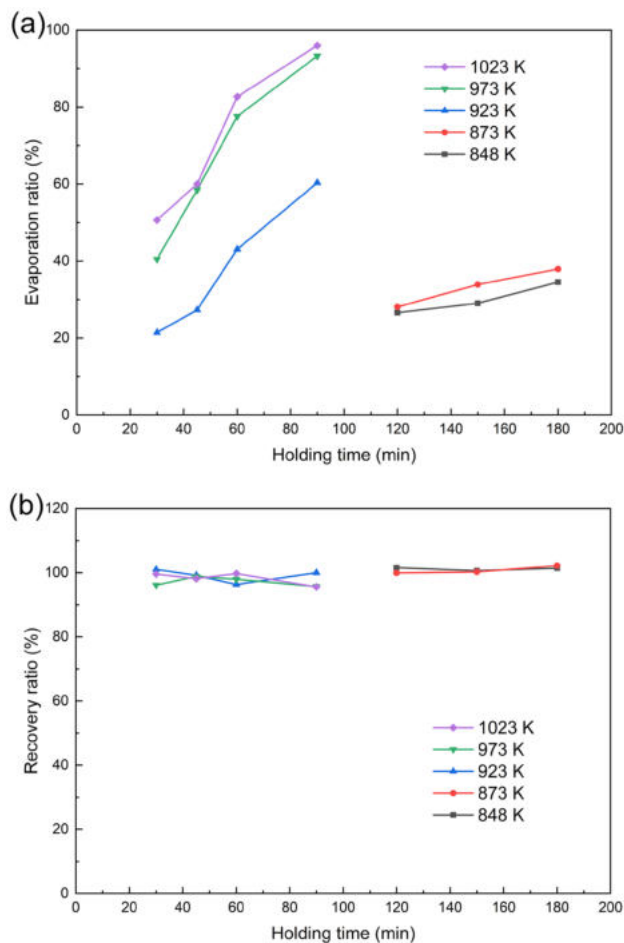
Fig. 6 The relationships between **a** the evaporation ratio and **b** the recovery ratio with the holding time at different temperatures. The recovery ratio refers to the proportion of the magnesium product obtained in the condenser chamber to the evaporated magnesium vapor

Fig. 7 The unremoved ratio of impurities Zn, Fe, Ca, Pb, Al, Cu, Ni, and Mn after vacuum distillation at heating temperatures of 848, 873, 923, 973, and 1023 K, respectively

collecting equipment and the control of condensing temperature and temperature gradient.

Conclusion

In summary, based on the theoretical criteria and a new self-designed distillation device, the process of purifying the commercial grade Mg into HP-Mg is studied through the one-step vacuum distillation method. In this process, the final product purity of nearly half a kilogram of 3N pure raw materials reaches 99.9958% (± 0.0034%), and the impurity behavior of eight impurities is analyzed. The new device has the advantages of high recovery efficiency, the lumpy condensed product, easy cleaning, and reusability. The results show that the average purification effect of vacuum evaporation is bigger than vacuum sublimation in the setup. However, no significant relationship between the steam jet temperature and the purity is observed in this study. Moreover, theoretical and experimental results jointly verify the difficulty sequence of impurity separation from the Mg base, which is Zn > Ca > Pb > Al > Cu > Ni. The close equilibrium vapor pressure of Zn and Mg is one of the reasons why Zn is the most difficult impurity to be removed from the Mg base; the other is that the separation coefficient of Zn is close to unity. In particular, unlike the easily removable impurity Mn, Fe occupies the second most difficult position to be

the separation coefficient and the gas–liquid equilibrium diagram, the order of reorganizing the experimental results, Zn > Ca > Pb > Al > Cu > Ni, is completely consistent with the theoretical criteria. It verifies the reliability of the separation coefficient β and the gas–liquid equilibrium diagram. However, unlike the easily removable impurity manganese, the final concentration of iron is unexpected, which located between zinc and calcium. Because the impurity iron should be removed via vacuum distillation [24], it can be reliably assumed that the abnormal behavior is caused by the contamination of the steel collection device [2] and the use of metal tools to take samples. In future work, this hypothesis can be clarified through comparative experiments with condensing devices made of other appropriate materials such as high-purity graphite. Further research directions can point to the interaction of impurity elements, the improvement of the condensation mechanism, and the recovery of magnesium vapor in liquid form, including the transformation of
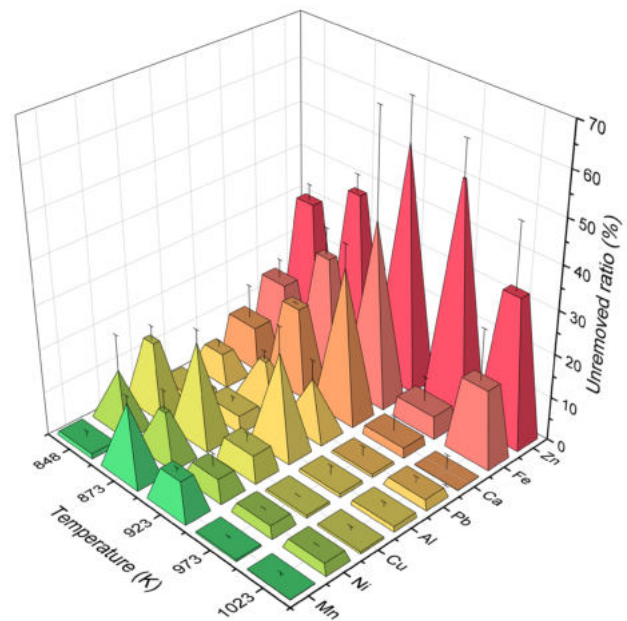
Table 3 The chemical analysis results of all impurities in raw materials and condensed Mg from condensation chamber after vacuum distillation experiments

Temperature (K)	Holding time (min)	Impurity concentration (ppm)									Mg purity (%)
		Zn	Ca	Pb	Mn	Al	Cu	Fe	Ni	Co	
	Raw material A (RA)	19.00	27.00	17.00	137.50	415.00	1.90	13.10	0.44	0.02	99.93690
	Raw material B (RB)	13.40	22.00	10.20	154.00	277.00	2.00	4.93	0.47	0.01	99.95160
848	120 (RA)	5.96	6.96	1.60	4.82	11.82	0.30	1.62	0.10	0.01	99.99668
	150 (RA)	5.89	2.55	1.02	1.28	4.81	2.27	2.05	0.12	0.01	99.99800
	180 (RA)	7.86	4.49	0.89	3.42	6.28	0.43	0.99	0.06	0.01	99.99756
873	120 (RA)	7.11	5.16	1.09	2.64	7.65	1.16	3.11	0.07	0.01	99.99720
	150 (RA)	8.03	14.53	0.80	3.58	10.24	0.41	1.41	0.05	0.01	99.99610
	180 (RA)	8.77	5.12	1.01	8.34	20.73	0.53	1.76	0.09	0.01	99.99537
923	30 (RB)	1.85	13.00	0.15	1.65	70.85	0.11	3.65	0.02	0.01	99.99087
	45 (RB)	4.00	13.50	0.45	4.53	102.00	0.22	4.00	0.05	0.01	99.98712
	60 (RB)	7.30	7.35	1.20	12.00	60.65	0.12	2.00	0.14	0.01	99.99092
	90 (RA)	15.30	1.50	8.65	75.85	365.00	1.74	13.40	0.33	0.01	99.95182
973	30 (RB)	14.50	2.62	0.37	0.02	3.00	0.01	1.33	0.03	0.02	99.99781
	45 (RA)	9.85	0.57	0.09	0.45	2.80	0.01	0.64	0.01	0.02	99.99856
	60 (RB)	11.50	0.01	0.02	0.19	23.58	0.01	0.25	0.01	0.01	99.99644
	90 (RA)	8.21	0.01	1.19	1.90	4.90	0.01	0.74	0.01	0.01	99.99830
1023	30 (RB)	12.20	0.01	0.29	2.27	10.74	0.08	1.38	0.05	0.01	99.99730
	45 (RB)	4.42	0.01	0.19	0.09	2.85	0.01	0.83	0.01	0.01	99.99916
	60 (RB)	7.43	0.22	0.05	0.04	2.20	0.01	2.20	0.04	0.01	99.99878
	90 (RB)	4.30	4.17	0.24	3.77	62.55	0.01	1.64	0.01	0.01	99.99233

removed. This may be caused by the contamination of the steel collection device and the sampling tools.

Declarations

Conflict of interest The authors declare that they have no known competing financial interests or personal relationships that could have appeared to influence the work reported in this paper.

References

1. Luo AA (2013) Magnesium casting technology for structural applications. J Magnes Alloy 1:2–22. https://doi.org/10.1016/j.jma.2013.02.002
2. Prasad A, Uggowitzer PJ, Shi ZM, Atrens A (2012) Production of high purity magnesium alloys by melt purification with Zr. Adv Eng Mater 14:477–490. https://doi.org/10.1002/adem.201200054
3. Peng Q, Huang Y, Zhou L, Hort N, Kainer KU (2010) Preparation and properties of high purity Mg–Y biomaterials. Biomaterials 31:398–403. https://doi.org/10.1016/j.biomaterials.2009.09.065
4. Froes FH, Eliezer D, Aghion E (1998) The science, technology, and applications of magnesium. JOM 50:30–34. https://doi.org/10.1007/s11837-998-0411-6
5. Xu W, Birbilis N, Sha G, Wang Y, Daniels JE, Xiao Y, Ferry M (2015) A high-specific-strength and corrosion-resistant magnesium alloy. Nat Mater 14:1229–1235. https://doi.org/10.1038/nmat4435
6. Song K, Pan FS, Chen XH, Zhang ZH, Tang AT, She J, Yu ZW, Pan HC, Xu XY (2015) Effect of texture on the electromagnetic shielding property of magnesium alloy. Mater Lett 157:73–76. https://doi.org/10.1016/j.matlet.2015.05.017
7. Li S, Yang X, Hou J, Du W (2020) A review on thermal conductivity of magnesium and its alloys. J Magnes Alloy 8:78–90. https://doi.org/10.1016/j.jma.2019.08.002

8. Pan H, Pan F, Yang R, Peng J, Zhao C, She J, Gao Z, Tang A (2014) Thermal and electrical conductivity of binary magnesium alloys. J Mater Sci 49:3107–3124. https://doi.org/10.1007/s10853-013-8012-3

9. Monteiro WA (2014) The influence of alloy element on magnesium for electronic devices applications—a review. Light Met Alloy Appl. https://doi.org/10.5772/58460

10. Zeng Z, Stanford N, Davies CHJ, Nie JF, Birbilis N (2019) Magnesium extrusion alloys: a review of developments and prospects. Int Mater Rev 64:27–62. https://doi.org/10.1080/09506608.2017.1421439

11. Staigera MP, Pietaka AM, Huadmaia J, Dias G (2006) Magnesium and its alloys as orthopedic biomaterials: a review. Biomaterials 27:1728–1734. https://doi.org/10.1016/j.biomaterials.2005.10.003

12. Song G, Atrens A (2003) Understanding magnesium corrosion—a framework for improved alloy performance. Adv Eng Mater 5:837–858. https://doi.org/10.1002/adem.200310405

13. Abidin NIZ, Rolfe B, Owen H, Malisano J, Martin D, Hofstetter J, Uggowitzer PJ, Atrens A (2013) The in vivo and in vitro corrosion of high-purity magnesium and magnesium alloys WZ21 and AZ91. Corros Sci 75:354–366. https://doi.org/10.1016/j.corsci.2013.06.019

14. Song GL, Atrens A (1999) Corrosion mechanisms of magnesium alloys. Adv Eng Mater 1:11–33. https://doi.org/10.1002/(SICI)1527-2648(199909)1:1%3c11::AID-ADEM11%3e3.0.CO;2-N

15. Höche D, Blawert C, Lamaka SV, Scharnagl N, Mendis C, Zheludkevich ML (2016) The effect of iron re-deposition on the corrosion of impurity-containing magnesium. Phys Chem Chem Phys 18:1279–1291. https://doi.org/10.1039/c5cp05577f

16. Birbilis N, King AD, Thomas S, Frankel GS, Scully JR (2014) Evidence for enhanced catalytic activity of magnesium arising from anodic dissolution. Electrochim Acta 132:277–283. https://doi.org/10.1016/j.electacta.2014.03.133

17. Duhaime P, Mercille P, Pineau M (2002) Electrolytic process technologies for the production of primary magnesium. Miner Process Extr Metall Rev 111:53–55. https://doi.org/10.1179/mpm.2002.111.2.53

18. Du J, Han W, Peng Y (2010) Life cycle greenhouse gases, energy and cost assessment of automobiles using magnesium from Chinese Pidgeon process. J Clean Prod 18:112–119. https://doi.org/10.1016/j.jclepro.2009.08.013

19. Tian Y, Wang L, Yang B, Dai Y, Xu B, Wang F, Xiong N (2020) Comparative evaluation of energy and resource consumption for vacuum carbothermal reduction and Pidgeon process used in magnesium production. J Magnes Alloy. https://doi.org/10.1016/j.jma.2020.09.024

20. Mohamed SR, Friedrich S, Friedrich B (2019) Refining principles and technical methodologies to produce ultra-pure magnesium for high-tech applications. Metals 9:85. https://doi.org/10.3390/met9010085

21. Inoue M, Iwai M, Matsuzawa K, Kamado S, Kojima Y (2003) Vacuum distillation refining and recycling of magnesium alloys. Mater Sci Forum 419–422:691–696. https://doi.org/10.4028/www.scientific.net/msf.419-422.691

22. Inoue M, Doi T, Aida T, Matsuki K, Kamado S, Kojima Y (2005) Vacuum distillation refining and extrusion process of magnesium. Mater Sci Forum 475–479:513–516. https://doi.org/10.4028/www.scientific.net/msf.475-479.513

23. Park J, Jung Y, Kusumah P, Dilasari B, Ku H, Kim H, Kwon K, Lee CK (2016) Room temperature magnesium electrorefining by using non-aqueous electrolyte. Met Mater Int 22:907–914. https://doi.org/10.1007/s12540-016-5605-9

24. Wang YC, Tian Y, Qu T, Yang B, Dai YN, Sun YP (2014) Purification of magnesium by vacuum distillation and its analysis. Mater Sci Forum 788:52–57. https://doi.org/10.4028/www.scientific.net/msf.788.52

25. Revel G, Pastol JL, Rouchaud JC, Fromageau R (1978) Purification of magnesium by vacuum distillation. Metall Mater Trans B 9:665–672. https://doi.org/10.1007/bf03257216

26. Papirov II, Kravchenko AI, Mazin AI, Shiyan AV, Virich VD (2015) Impurity distribution in a magnesium sublimate. Inorg Mater 51:563–565. https://doi.org/10.1134/S0020168515060126

27. Mizuhara K, Inoue M, Aida T, Matsuzawa K, Aoyagi N, Miura H (2020) Preparation of ultra high purity magnesium sheet by vacuum distillation and extrusion. Trans Gigaku 7:07004-1–07004-7. https://doi.org/10.34468/gigaku.7.1_07004-1

28. Rodushkin I, Ruth T, Huhtasaari Å (1999) Comparison of two digestion methods for elemental determinations in plant material by ICP techniques. Anal Chim Acta 378:191–200. https://doi.org/10.1016/S0003-2670(98)00635-7

29. Comparison of ICP-OES and ICP-MS for trace element analysis. https://www.thermofisher.com/de/de/home/industrial/environmental/environmental-learning-center/contaminant-analysis-information/metal-analysis/comparison-icp-oes-icp-ms-trace-element-analysis.html

30. Lam RKF, Marx DR (1996) Ultra high purity magnesium vacuum distillation purification method. US Patent 5582630A

31. Tayama K, Kimura S (2003) High purity metals, process and apparatus for producing them by enhanced purification. European Patent 1335030A1

32. Tian Y, Zhang X, Qu T, Lyu F, Du H, Shi L, Yang B, Dai Y (2021) Technical research on vacuum distillation to purify magnesium to 99.99% purity. Mater Res Express 8:056506. https://doi.org/10.1088/2053-1591/abdf12

33. Wegmann C, Löffler J, Uggowitzer P, Becker M, Feichtinger H (2017) Process and apparatus for vacuum distillation of high-purity magnesium. US Patent 9677151B2

34. Du X, Zeng Z, Yuan H, Li H, Xue Q, Jia J (2010) High vacuum in situ refining method for high-purity materials and an apparatus thereof. US Patent 7753987B2

35. Dai YN, Yang B (2009) Vacuum metallurgy of nonferrous metals. Metallurgical Industry Press, Beijing

36. Liang YJ, Che YC (1993) Handbook of thermodynamic data for inorganic substances. Northeast University Press, Lebanon, pp 513–528

37. Hultgren R, Desai PD, Hawkins DT, Gleiser M, Kelley KK (1973) Selected values of the thermodynamic properties of binary alloys. ASM, Metals Park

38. Xiong N, Tian Y, Yang B, Xu BQ, Liu DC, Dai YN (2018) Volatilization and condensation behaviours of Mg under vacuum. Vacuum 156:463–468. https://doi.org/10.1016/j.vacuum.2018.08.014

39. Han J, Fu D, Guo J, Ji Z, Dou Z, Zhang T (2020) Nucleation and condensation of magnesium vapor in argon carrier. Metals 10:1441. https://doi.org/10.3390/met10111441

40. Yang B, Liang D, Xiong N, Tian Y, Xu BQ, Dai YN (2021) Effect of crystallization on purity of volatile metallic magnesium prepared from a one-step multi-region condensation process under vacuum condition. J Magnes Alloy. https://doi.org/10.1016/j.jma.2021.08.008

Authors and Affiliations

Neng Xiong[1] · Semiramis Friedrich[1] · Seifeldin R. Mohamed[1] · Ivan Kirillov[1] · Xiaozhou Ye[1] · Yang Tian[2,3] · Bernd Friedrich[1]

✉ Semiramis Friedrich
   SFriedrich@ime-aachen.de

✉ Yang Tian
   emontian@hotmail.com

[1] IME Institute of Process Metallurgy and Metal Recycling, RWTH Aachen University, 52056 Aachen, Germany

[2] National Engineering Research Center of Vacuum Metallurgy, Kunming 650093, China

[3] School of Metallurgy and Energy Engineering, Kunming University of Science and Technology, Kunming 650093, China